

A review for antenna performance enhancement using metasurface structures

Review
Article

Mohamed El-Sewedy, Mahmoud A. Abdalla

Department of Electronic Engineering, Military Technical College, Cairo, Egypt

Keywords:

Anomalous reflection, anomalous refraction, generalized Snell's law, high gain, Metasurface, mutual coupling reduction, RCS reduction.

Corresponding Author:

Mohamed El-Sewedy, Department of Electronic Engineering, Military Technical College, Tel: 01013073107, Email: mohamed.elsewedy@ieec.org

Abstract

Metasurfaces (MS) have recently attracted a lot of attention due to their ability to manipulate electromagnetic characteristics. The metasurface is constructed from two-dimensional scatterers (metallic and dielectric) which provide simplicity in fabrication and flexibility for integration with other systems. The metallic metasurface unit cells and dielectric metasurface unit cells have a length of sub-wavelength. Most essential ideas of metasurfaces are directly borrowed from antenna array theories such as reflectarray and transmitarray. On the other hand, progress in metasurfaces has aided and accelerated the development of antennas. Metasurface can be used to achieve an increase of the gain of antenna depending on the hyperbolic phase distribution of the metasurface unit cell which constructs the focusing metasurface. Also, the metasurface can be used to achieve RCS reduction, mutual coupling reduction, frequency scanning, multibeam generation, and end-fire antenna.

I. INTRODUCTION

Metasurfaces are periodic structures with the thickness and the periodicity of the individual elements is small relative to the operating wavelength. There are two important subclasses, metasurfaces that are called metafilms which is an array of isolated scatters as shown in Fig.1(a), and a metasurface with fishnet topology which is called metascreens as shown in Fig.1(b). They are regarded as periodically spaced apertures in a reflective screen^[1]. In this portion, an approach for the specific characterization of a metafilm based on an inversion of its coefficients of reflection and transmission to obtain the susceptibility of the surface is presented in^[2,3]. A metafilm's reflection (R) and transmission (T) coefficients were extracted in^[4] for

both TE and TM polarized plane waves.

II. GENERALIZED LAWS OF REFLECTION AND REFRACTION

If an electromagnetic plane wave meets two homogeneous media containing different refractive indices, it is divided into a reflection ray that spreads back to the first medium and a transmitted beam that spread to the second medium. The coefficients of reflections and transmissions and their directions are determined by the continuity of field components at the boundaries and are given according to Fresnel equations and Snell's law. The implementation of a phase shift at the interface between two media, known as phase discontinuity, enables us to review the laws of reflection and refraction by using Fermat's principle^[5].

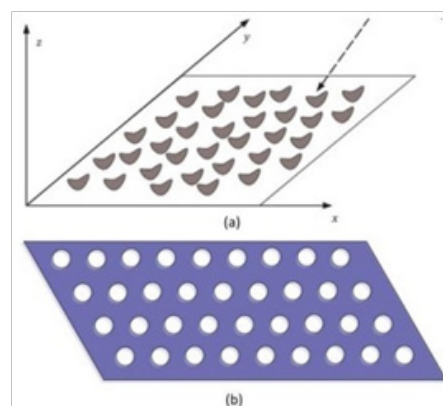


Fig. 1: (a) metafilms, (b) metascreen^[1].

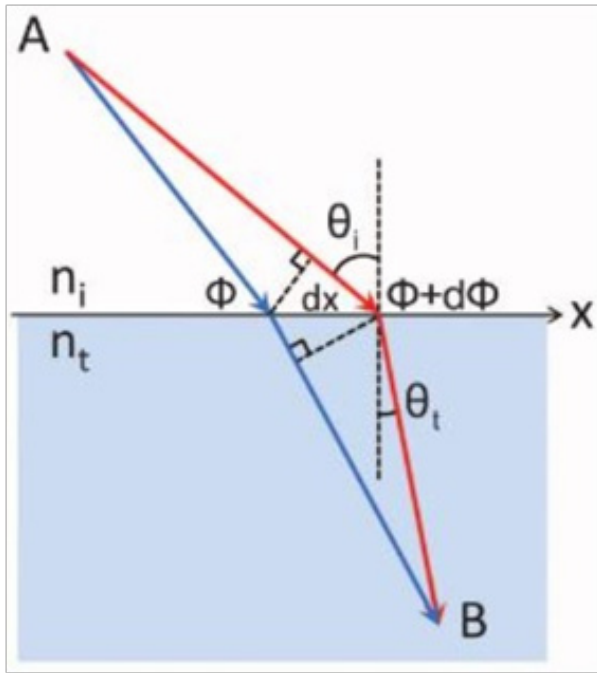


Fig. 2: Schematic view of generalized Snell's law of refraction^[5].

If we have an incident plane wave with angle θ_i , by assuming the two paths indicated in Fig. 2 are close to the actual light path, the phase difference between two paths will be zero as^[5]:

$$[k \cdot n_i \sin(\theta_i) dx + (\varphi + d\varphi)] - [k \cdot n_t \sin(\theta_t) dx + \varphi] = 0 \quad (1)$$

Where $\varphi + d\varphi$ and φ are the phase discontinuities at the interface between them, n_i and n_t are the refractive indices of the two media, θ_t is the angle of refraction, dx is the distance between two points at the interface and $k_0 = 2\pi/\lambda_0$.

The previous equation leads to generalized Snell's law of refraction if the phase gradient is constant along with the interface between two media as^[5]:

$$n_t \sin(\theta_t) - n_i \sin(\theta_i) = \frac{\lambda_0}{2\pi} \frac{d\varphi}{dx} \quad (1)$$

Equation (2) means the refracted beam has an arbitrary direction, given a constant phase discontinuity gradient is applied along with the interface. The amount of energy in the anomalously reflected and refracted beams is controlled by the separation between the resonators.

There are anomalous refraction phenomena caused by metamaterial which depends on either anisotropic dielectric permittivity with different signs of permittivity tensor component transverse or along to the surface or the negative dielectric permittivity and negative

magnetic permeability^[6, 7]. There is a must to differ from the above anomalous refraction and that is done by phase discontinuity.

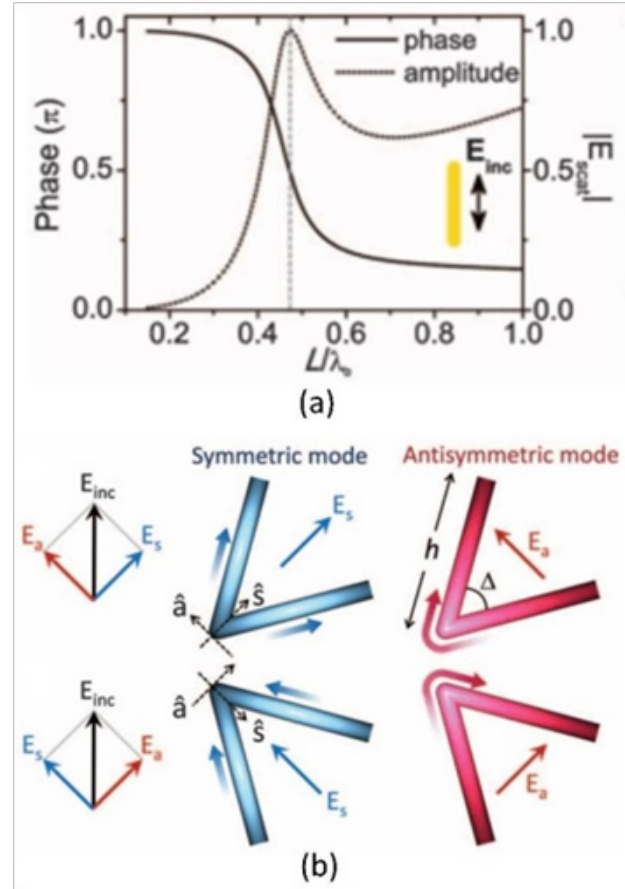


Fig. 3: (a) amplitude and phase of scattered wave from perfect electric conductor rod antenna. (b) V-shaped antennas to achieve full phase range coverage^[5].

The design of phase discontinuity along the interface can be done by designing the shape of the resonators in the designed array and their frequency response. The resonators may be determined as electromagnetic cavities^[8], nano-scatterers^[9], and plasmonic antennas^[10]. Plasmonic antennas have the advantage of the ease of fabrication planar antennas and have widely variable optical properties.

The calculated amplitude and phase of the scattered wave from the perfect electric conductor rod antenna are shown in Fig. 3 (a). In order to provide full control of wavefront, phase shift must cover the range from 0 to 2π . V-shaped antennas are designed to achieve full phase range coverage as shown in Fig. 3 (b). The supercell is consisting of eight V-shaped antennas as in Fig. 4. The Finite-difference time-domain simulation of the supercell is shown in fig z which clarifies the amplitudes of all cells in the supercell are nearly equal and the phase increments by $\pi/4$.

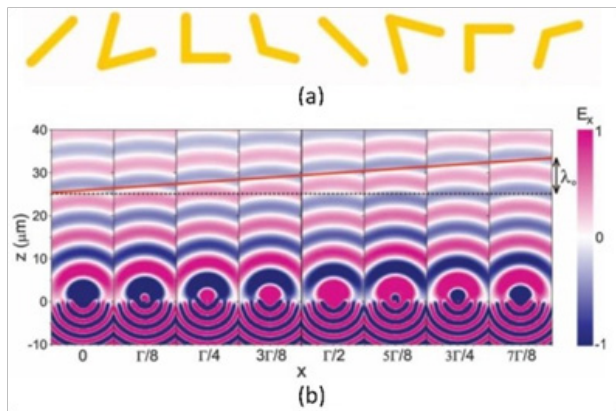


Fig. 4: (a) V-shaped supercell that construct the supercell. (b) Finite difference time domain of the super cell^[5].

III. REFLECT ARRAYS BASED ON ANOMALOUS REFLECTION METASURFACE

As mentioned in the previous section for generalized Snell's law, an array of subwavelength metasurface atoms with variable shapes and dimensions can construct a reflection phase gradient metasurface. From point of view of the antenna, when a plane wave is an incident on the reflection phase gradient metasurface, each individual cell acts as a transmitting antenna that radiates the reflected wave with variable phase.

The reflectarray theory and its techniques make the progress in reflectarray metasurface are fast because the main concept of reflectarray antennas is equivalent to the concept of anomalous reflection metasurface^[11]. When metasurface is constructed for anomalous reflection, there is a must for using the metallic ground plane to ensure high reflectivity and prevent the wave from penetrating the structure. There is a lot of metasurface unit cells have been developed such as dipoles and patch cavities^[12,13,14-17].

In^[18], the metasurface is designed to achieve single polarized anomalous reflections and introduce that a gradient index metasurface can convert a plane wave to surface wave with nearly 100% efficiency by using H-shaped metasurface antennas and metallic ground plane separated by dielectric as shown in Fig. 5 (a), (b). This proves that the reflection phase gradient metasurface can compensate for the mismatch between plane wave and surface wave for any incident angle greater than the critical angle.

Also, anomalous reflection metasurface is used to achieve dual-polarization and dual-mode orbital momentum vortex beam by using cross-dipoles^[15]. The layer of the metasurface is consists of $M \times N$ elements. And the feed antenna produces an incident wave at position R_f as shown in Fig. 6 (a). The structure of the cross dipole metasurface element is shown in Fig.6 (b) and the results of its phase and magnitude are shown in Fig.6 (c), (d) with different L_v of the cross dipole at 5.8 GHz. The phase distribution of x-polarization and y-polarization are shown in Fig. 6 (e), (f) respectively which proves the concept of

anomalous reflection metasurface can be utilized to obtain a dual-polarization vortex beam.

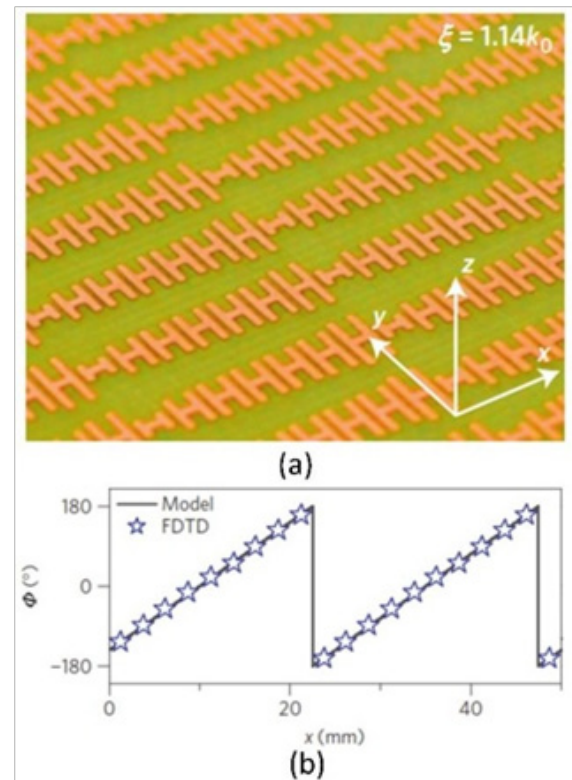


Fig. 5: (a) H-shaped antennas to convert plane wave to surface wave, (b) the reflection phase profile for phase gradient metasurface along X-axis^[18].

IV. TRANSMIT ARRAYS BASED ON ANOMALOUS REFRACTION METASURFACE

The reflected wave that is generated by phase gradient (PGM) metasurface can be controlled as deduced by generalized Snell's law as shown in Fig. (7). In anomalous refraction, the transmission phase must be customized similar to anomalous reflection MS besides the transmission magnitude must be near unity for getting high-efficiency refraction.

In^[19], high-efficiency anomalous refraction and polarization conversion is realized by using an ultrathin metasurface with different rotation angles based on Pancharatnam-Berry (PB) law. the unit cell that is used achieve thickness reduction, focusing, and high transmission efficiency. The planar array and the unit cell are shown in Fig. (8).

Recently, researchers use techniques of multilayers of metasurface to obtain higher efficiency than a single metasurface layer^[20,21]. In^[21], three cascade metasurfaces layers were used to achieve three different functions to provide a full function of wave control as shown in Fig. 9 (a).

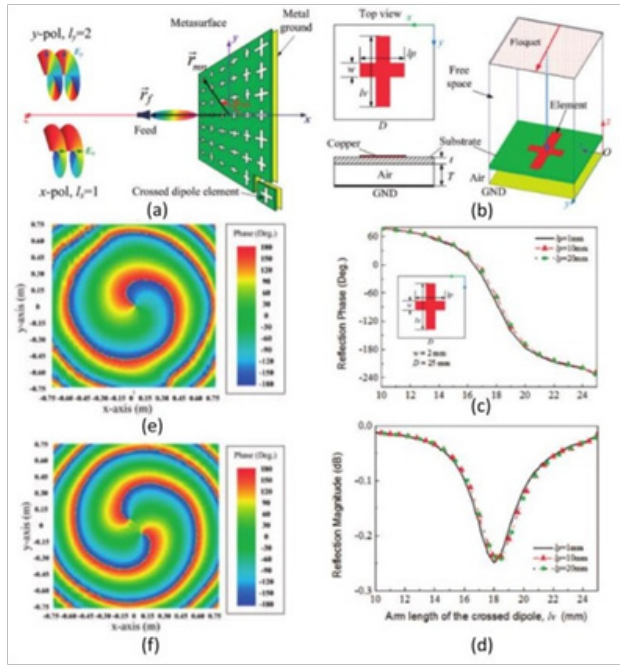


Fig. 6: (a) Anomalous reflection metasurface layer to achieve dual polarization and dual mode orbital momentum vortex. (b) Cross-dipole metasurface unit cell geometry. (c) The reflection phase of the unit cell. (d) The reflection magnitude of the unit cell. (e) The x-pol phase distribution of the metasurface layer. (f) The y-pol phase distribution of the metasurface layer^[15].

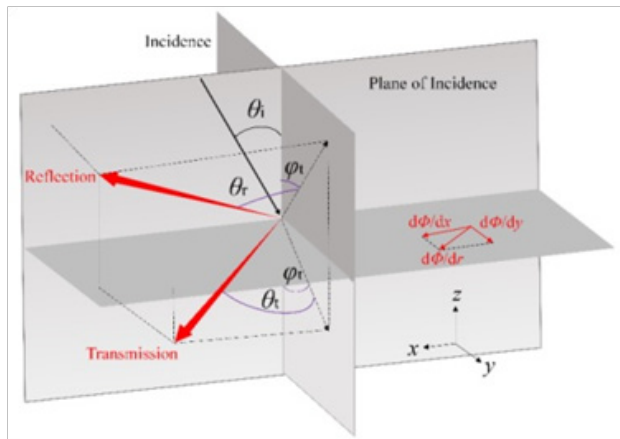


Fig. 7: A phase gradient metasurface that causes anomalous reflection and refraction^[5].

The wave is incident from +z direction upon the cascaded layers. The first layer is called meta-mirror and it reflects the incident wave (at normal direction) to an angle of 45 degrees from the normal at 5 GHz. In general, the first layer is used to prevent the waves from the radiation in the backward direction and reflects the wave to any angle in the forward direction only as shown in Fig. 9 (b). The second layer has a function of wave absorption at 6 GHz. The elements of this layer are helixes as depicted in Fig. 9 (c). The third layer of the metasurface is used to focus the incident radiation at a frequency of 3.9 GHz as shown in

Fig. 9 (d). besides the construction of the above-mentioned layer (helixes), multi-layers metasurface is designed as multilayers of patches^[22,23] and dipoles^[24].

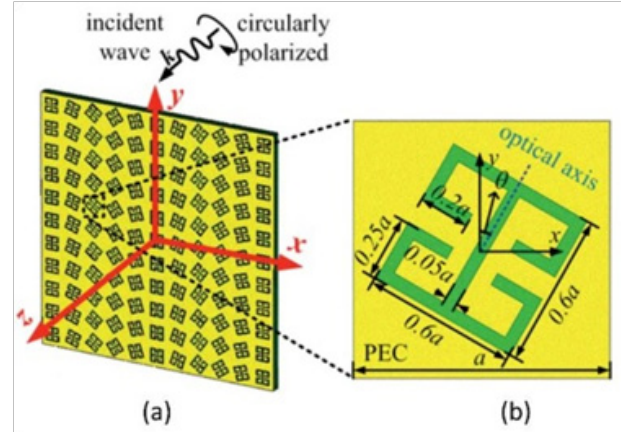


Fig. 8: (a) Schematic view of the ultrathin metasurface layer with different rotation angles based on Pancharatnam-Berry (PB) law. (b) the detailed dimensions of the metasurface unit cell^[19].

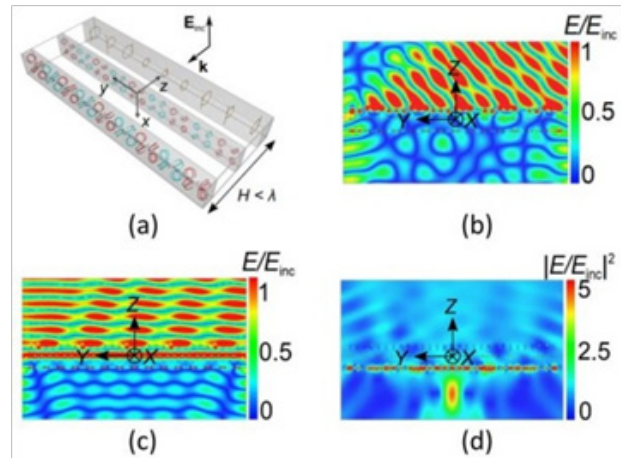


Fig. 9: (a) Three cascade metasurfaces layer [21]. Electric field distribution at (b) 5 GHz, (c) 6 GHz and (d) 3.9 GHz.

V. HIGH DIRECTIVE ANTENNAS

Directivity is very important especially in wireless applications to focus the radiated power in a certain direction. The traditional method to get high directivity is using a planar array with a metallic ground plane as a reflector but there is a problem of large and bulky profile addition to the complexity of the feeding network. So, researchers turned to the usage of metasurface trying to solve the problems of traditional methods.

In general, metasurface (MS) layers have been used to design new PRS functionalities in Fabry-Pérot cavity antenna thanks to its unique characteristics [25], [26]. Fabry-Pérot cavity (FPC) antennas have a high gain and high directivity but have the advantage of being simple in structure, easy to fabricate, easy to integrate with the

system, and inexpensive. FPC antenna is formed of the main emitting source with a background PEC layer, and a partially reflecting surface (PRS)^[27]. In^[28], coding metasurface is introduced to create an FPC antenna with high gain by achieving low scattering over the band of frequency from 8 GHz to 12 GHz by re-emitting the electromagnetic waves in all directions without effect on the radiation characteristics. Two layers of square unit cells make up the coding metasurface. printed on a dielectric material substrate. the upper one is used to structure coding metasurface while the bottom one is used as PRS as shown in Fig. (10).

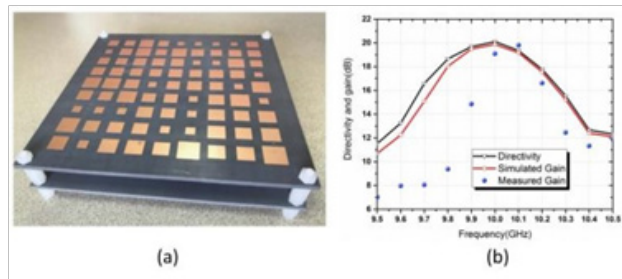


Fig. 10: (a) Geometry of FPC antenna using coding metasurface principle. (b) The directivity and the gain of the FPC antenna^[28].

After introducing the generalized Snell's law, focusing effect of phase gradient metasurface (PGM) had great interest. The layer of PGM is used to realize a high gain transmitting lens antenna by converting the quasi-spherical wave that is emitted by the feeding source antenna to a plane wave. Thus, the beam of the feeding source antenna becomes narrower compared with the non-exist of the PGM layer and hence the gain is increased^[29]. In the previously mentioned reference, the feeding source antenna is a patch antenna and the PGM unit cells are circular cells with a different radius that convert the spherical waves to plane waves as shown in Fig 11 (a). The gain is enhanced by using the previously described method by 11.6 dB as shown in Fig 11 (b).

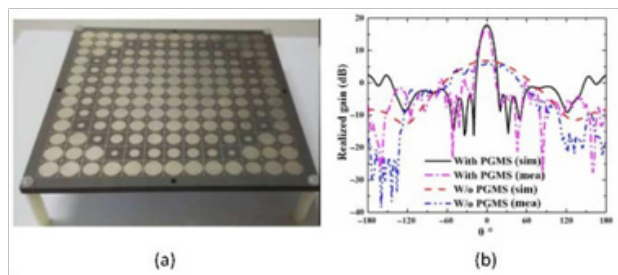


Fig. 11: (a) Fabricated phase gradient metasurface focusing antenna. (b) Measured far field radiation pattern of PGMS lens antenna^[29].

Another technique for increasing the gain of the antenna is using phase compensation metasurface^[30,31,32]. In^[30], the authors depend on Hygens' principle^[33] to compensate the out-of-phase characteristics of the radiated waves from the feeding source antenna by employing inductive elements and capacitive elements which construct the metasurface unit cell as shown in Fig. 12 (a).

This phase compensation metasurface unit cell converts the radiated spherical waves from the patch antenna (source antenna) to an in-phase plane wave and hence the gain and bandwidth of the antenna are enhanced as depicted in Fig. 12 (b).

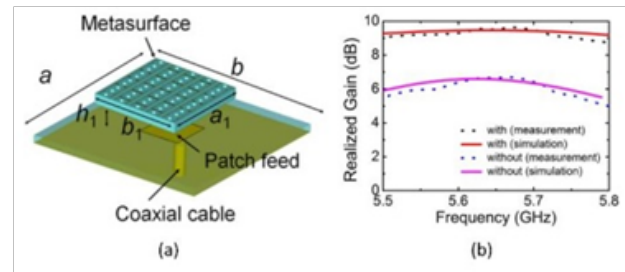


Fig. 12: (a) Phase compensated metasurface's schematic view. (b) Realized gain of the metasurface unit cells^[30].

Also, Huygens' metasurface is used to realize high gain antennas. A dual-layer Huygens' unit cell based on offset electric dipole pair (OEDP) was used in^[69]. The main design has two steps, the first step is the generation of the Rotman lens and the second is using the Huygens' metasurface layer for enhancement of the antenna gain as shown in Fig. (13). The realized antenna has a wideband from 28 GHz to 32 GHz with 24.4 dBi maximum gain.

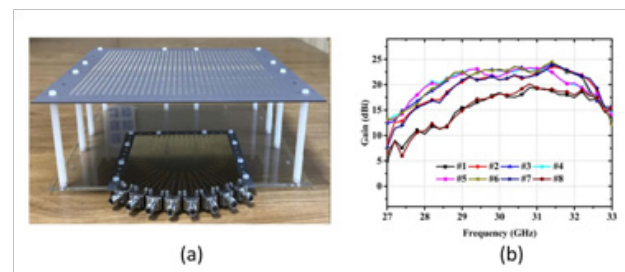


Fig. 13: (a) Fabricated antenna with Huygens' metasurface layer. (b) Realized gain^[69].

VI. LOW RCS ANTENNA

In recent years, for stealth technology, the reduction of electromagnetic fields dispersed from metallic objects has sparked a lot of attention. The decrease of radar cross-sections (RCS) is the most remarkable aspect of the technology of secrecy. There is a lot of metasurface techniques to reduce monostatic and bistatic radar

cross-section listed as follows, polarization conversion metasurfaces^[34,35], absorptive metasurface, and beam deflection^[36,37], phase gradient metasurface^[38] and coding metasurface^[39].

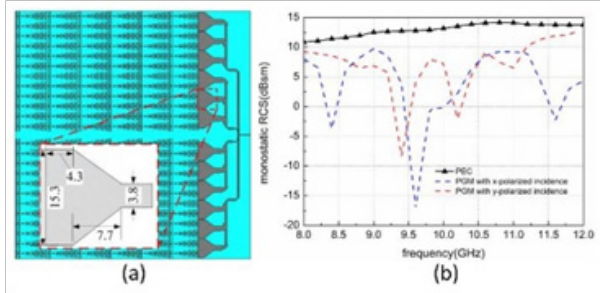


Fig. 14: (a) Geometry of RCS reduction technique. (b) Measured x-polarized and y-polarized monostatic RCS^[38].

In^[38], phase gradient metasurface is used to achieve RCS reduction. H-shaped elements with different dimensions are used to construct phase gradient metasurface to steer the beam from 16.4° to 12.7°. The designed metasurface is coplanar with parallel plate waveguide feeder and couples guided waves in feeding source into radiation waves which in turn deviate the incident wave into a different direction and finally reduce RCS as shown in Fig. 14 (a). The designed antenna has a peak RCS reduction of 30 dB for x-polarized and 22 dB for y-polarized illuminated waves as shown in Fig. 14 (b).

Also, RSC reduction can be realized by using two metasurface unit cells arranged in chessboard configuration as in^[40,42]. In^[43], two different metasurface artificial magnetic conductors (AMC1 and AMC2) are used to achieve destructive interference between the reflected waves from them.

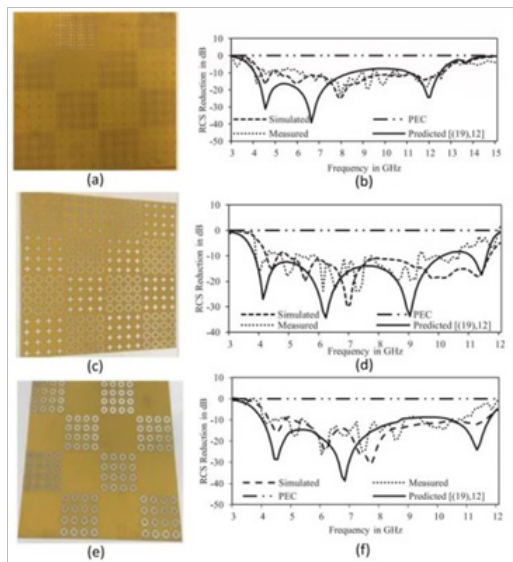


Fig. 15: (a) JC large-small elements configuration. (b) Mono static RCS of JC large-small configuration. (c) Simple cross-slotted cross elements configuration (d) Mono static RCS of Simple cross-slotted cross configuration. (e) Slotted cross with 'L' corner elements configuration. (f) Mono static RCS of Slotted cross with 'L' corner^[43].

The required phase difference between the reflected waves from AMC1 and AMC2 should be $180^{\circ} \pm 37^{\circ}$ in order to achieve a 10 dB reduction in RCS. The three configurations (JC large-small, simple cross-slotted cross, and Slotted cross with 'L' corner) and their corresponding RCS reduction are shown in Fig15 (a)-(f). In^[70], broadband RCS reduction was achieved by using multilayer Jerusalem cross pattern and cross-slot pattern metasurface unit cells. A -10 dB RCS reduction was achieved over a frequency band from 3.5 to 11.5 GHz as shown in Fig. (16).

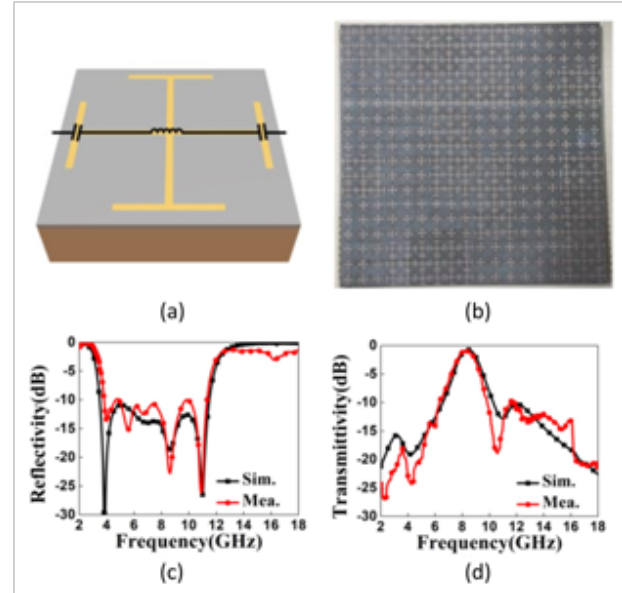


Fig. 16: (a) metasurface unit cell. (b) Fabricated prototype. (c) Reflectivity. (d) transmittivity^[70].

A comparison table which indicates the advantage of using metasurface technique than traditional techniques for RCS reduction applications is shown below in Table 1.

Table 1: A comparison between Metasurface techniques and other non-Metasurface techniques (low RCS antenna)

Ref.	Substrate thickness in mm	relative permittivity	RCS reduction band in GHz
71 (non-metasurface)	6.35	2.2	4.2-7.8 (60%)
72 (non-metasurface)	6.35	2.2	8.41-10.72 (27%)
73 (non-metasurface)	11 vacuum + 0.5 substrate	3.48	3.77-10.41 (91.5%)
43 (metasurface)	5 vacuum + 1.57 substrate	4.3	4.3-12.6 (98%)
70 (metasurface)	9 vacuum + 0.25 substrate	2.65	3.5-11.5 (NA)

VII. MUTUAL COUPLING REDUCTION OF ANTENNA

There is a great interest to reduce mutual coupling between antenna elements because the high coupling between antenna elements has a harmful effect on antenna parameters. High mutual coupling degrades the radiation efficiency of the antenna and affects the input impedance besides its effect on the S-parameters (reflection coefficient and transmission coefficient). Also, mutual coupling makes a deviation in the radiation pattern of the antenna^[44].

There are various techniques to reduce mutual coupling between elements of antenna such as defective ground structure (DGS)^[45], electromagnetic bandgap (EBG)^[46], and artificial magnetic conductor (AMC)^[47]. The main role of the previously mentioned techniques is to suppress the surface wave and hence realize the reduction of mutual coupling. Using traditional techniques has a problem of reducing the mutual coupling between elements only in one direction besides the disadvantages of narrow bandwidth. So, the mutual coupling reduction by using metasurface is introduced to overcome these problems.

In 2015, Bernety introduced a novel method to reduce mutual coupling reduction between two strip dipole antennas^[48]. The authors depend on using a technique of mentle cloaking metasurface^[49,50] to make the strip dipoles is invisible to each other and hence the mutual coupling reduction was achieved.

In^[51], an array of split ring metasurface is integrated between two circular dielectric resonator antennas to reduce the mutual coupling reduction for the millimeter-wave band. The metasurface layer is acting as a shield between the antenna elements as shown in Fig. 17 (a). The used split ring metasurface layer achieves an isolation level between -30 dB to -46 dB over the resonant frequency of DRA MIMO antenna over the frequency band from 59.3 GHz to 64.8 GHz as shown in Fig. 17 (b).

The metasurface array layer is mounted between the radiated antenna elements in^[51], while in^[52] an additional metasurface superstrate layer is mounted above the main feeding antenna substrate with a height of $0.2 \lambda_0$ to provide E-plane and H-plane mutual coupling reduction as shown in Fig. 18 (a)-(d). Two traditional patch antenna is used to radiate the power with spacing from edge to edge of $0.023 \lambda_0$ and the metasurface unit cell are a square slot. The metasurface superstrate is consists of a 4×5 array of unit cells. The maximum reduction in mutual coupling is 40 dB at 3.5 GHz.

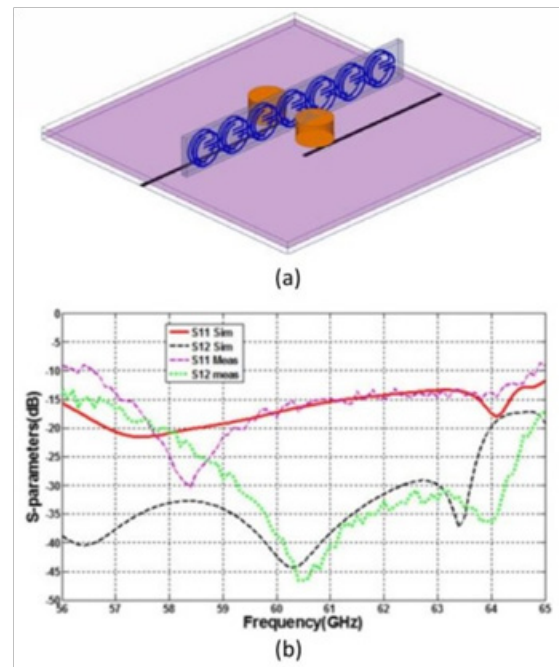


Fig. 17: (a) Configuration of DRA with metasurface to reduce mutual coupling^[51] (b) The simulated and measured S-parameters of DRA.

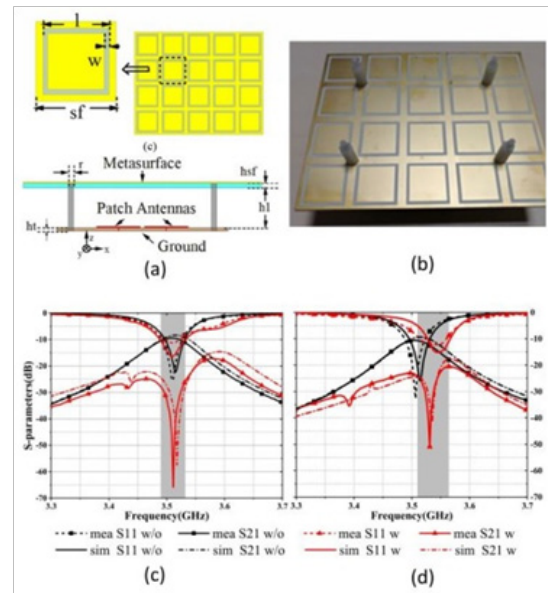


Fig. 18: (a) Mutual coupling reduction by using square slots [52] (top view and side view of antenna). (b) The fabricated prototype. (c) The measured s-parameter for E-plane. (d) The measured s-parameter for H-plane.

In^[53], instead of using one superstrate as in^[52], two superstrate layers of metasurface are used to provide mutual coupling reduction between 4×4 antenna array for MIMO applications as shown in Fig. 19.

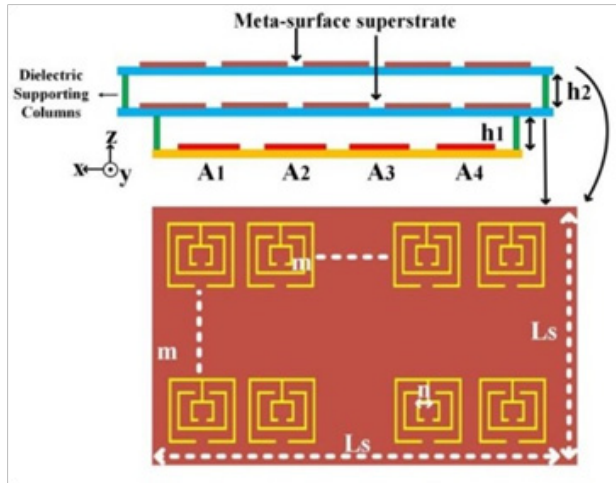


Fig. 19: The configuration of using two metasurface superstrate to provide mutual coupling reduction^[53].

A comparison table which indicates the advantage of using metasurface technique than traditional techniques for mutual coupling reduction applications is shown below in table II

Table 2: A comparison between metasurface techniques and other non-Metasurface techniques (mutual coupling reduction)

Ref.	Frequency (GHz)	Edge-to-edge Spacing	Max Reduction in (dB)
74 (PCR)	3.5	0.07λ	26.2
75 (ACPS)	5.8	0.03λ	45.2
76 (CSRR)	3.6	0.125λ	27
52 (metasurface)	3.51	0.023λ	55
70 (metasurface)	60.4	NA	46.5

VIII. FREQUENCY SCANNING METASURFACE ANTENNA

As mentioned in the above sections, the metasurface can be used to improve the characteristics of the antenna such as improving the directivity, gain, reduction of the radar cross-section and mutual coupling reduction besides it is used to construct reflectarrays and transmitarrays. Metasurfaces can also be used to provide frequency scanning by using phase gradient unitcells which have the property of providing coupling of spoof surface plasmon polariton (SSPP) besides decoupling it^[54,55]. In^[56], the authors used a reflective phase gradient metasurface to achieve frequency scanning for the planar antenna.

The antenna is composed of transmissive phase gradient metasurface unitcells which were put above SSPP guided wave structure as shown in Fig. 20 (a).

The planar antenna had fed with a rectangular waveguide. The planar antenna has a wideband frequency scanning from 7 GHz to 10 GHz with a total efficiency of 90 % as concluded from the radiation pattern which shown in Fig. 20 (c), (d). Also, in^[57], a supercell that consists of six-unit cells was used to construct the phase gradient metasurface which in turn it provides a frequency scanning from 8.8 GHz to 10.7 GHz as shown in Fig. 21.

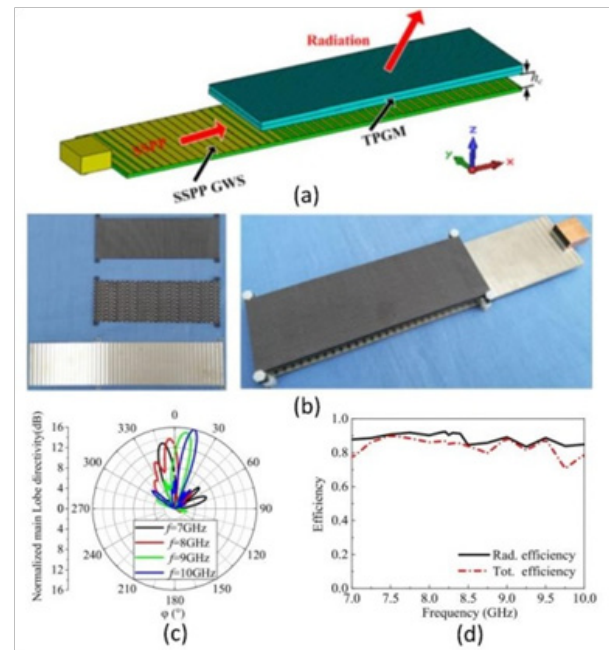


Fig. 20: (a) schematic view of transmissive phase gradient metasurface unit cells which is above SSPP guided wave structure. (b) the fabricated antenna. (c) radiation pattern at different frequencies. (d) the total efficiency and the radiated efficiency of metasurface antenna^[56].

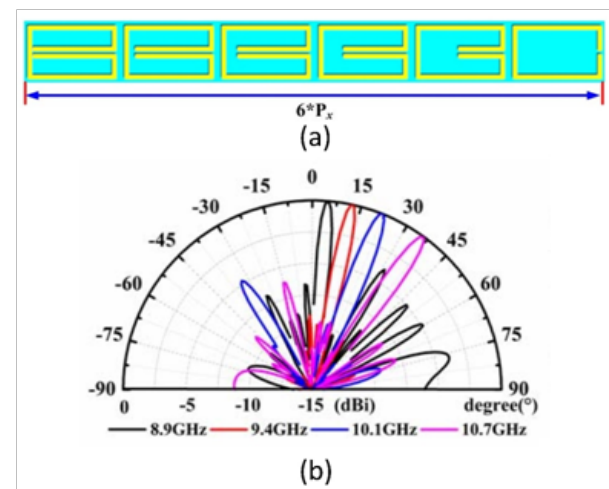


Fig. 21: (a) The geometry of the metasurface supercell which consists of six-unit cells. (b) the radiation pattern which declare the different angles of different frequencies^[57].

Another technique for providing frequency scanning was introduced in^[58] by using spatial angular filtering metasurface which is shown in Fig. 22(a). When the C-shaped phase gradient metasurface is illuminated by TE-polarized plane waves with various incident angles, the metasurface unit cells will generate variable wavelength unit cells will generate variable wavelength energies. The introduced tapered waveguide provides frequency scanning from 15.9 GHz to 16.8 GHz with different angles as shown in Fig. 22(b).

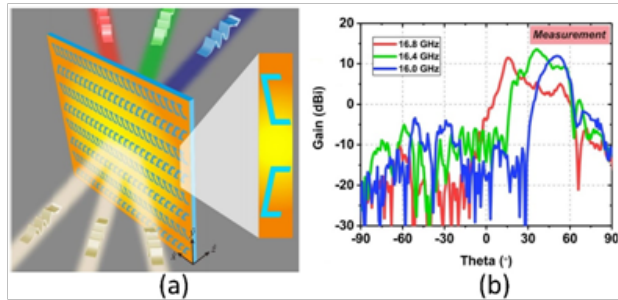


Fig. 22: (a) The configuration of using spatial angular filtering metasurface layer. (b) the radiation characteristics after using metasurface layer^[58].

IX. MULTI-BEAM METASURFACE ANTENNA

Depending on the advantage of metasurface having a great control in manipulating the radiated waves as mentioned in section II, the multi-beam generation can be achieved by using metasurface unit cells^[59,60]. As introduced in^[61], to manipulate and construct a flexible radiation pattern, a low-profile planar array antenna was introduced by using coding metasurface unit cells. The coding metasurface unit cell was arranged in between the radiating patches of the array to obtain good radiation characteristics and reduce the scattering from the microstrip array as shown in Fig. 23(a). After using the coding metasurface unit cells, the coding array become have fourbeams at different angles as shown in Fig. 23(b) besides, the gain was still not affected.

Also, a dual-polarized multi-beam metasurface antenna was introduced in^[62]. An array of the subwavelength slot-shaped unit cell was used to construct the metasurface array. The multi-beam forming function is achieved without using phase-shifting circuits. The introduced metasurface antenna has three main lobes in three different directions as shown in Fig. 24.

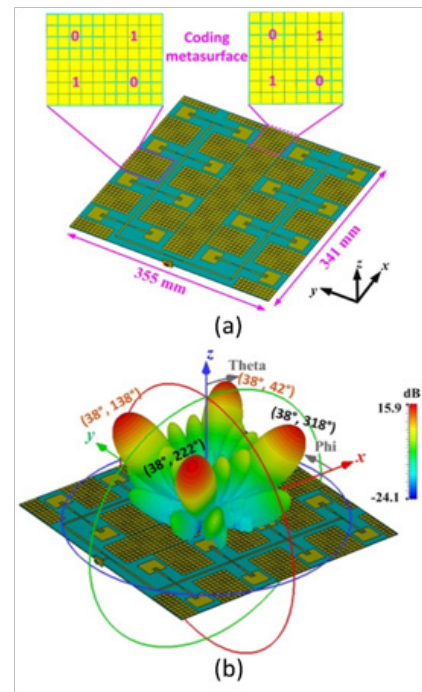


Fig. 23: (a) The geometry of antenna array with coding metasurface in between the array patches. (b) 3-D radiation pattern of the array antenna with metasurface to generate multi-beam^[61].

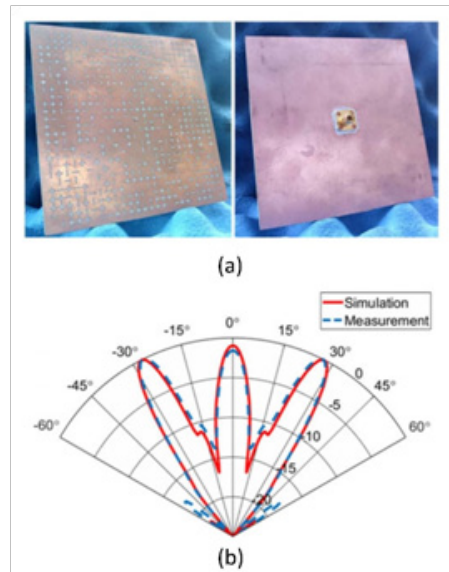


Fig. 24: Dual polarized multi-beam metasurface antenna (a) the antenna geometry. (b) the radiation pattern^[62].

X. END-FIRE METASURFACE ANTENNA

In the last few years, end-fire antennas have had a great interest due to their numerous applications in aeroplanes and unmanned aerial vehicles (UAV)^[63-65]. Recently, introducing metasurface to be used in end-fire antenna have attracted a lot of attention because of its advantage of simplicity in fabrication, minimal cost, low profile and lightweight^[66,67].

In^[67], a metasurface principle was illustrated and implemented in the construction to achieve a low profile and wideband end-fire antenna. The metasurface construction is divided into two parts as shown in Fig. 23 (a). In the first part, two rows of the same size rectangular metasurface unit cell were used to improve the impedance matching. The second part is fourteen rows of metasurface unit cells with variable sizes to provide the property of wideband and

low profile. The metasurface unit cells rows were fed by surface wave launcher as depicted in Fig.23 (a). The profile size of the metasurface end-fire antenna was 0.065λ and the fractional bandwidth was 125%.

A quasi-Yagi antenna that works in the UHF frequency band was presented in^[68]. The antenna was printed on a textile substrate which can be adopted to take the shape of the arm. The radiation pattern of the quasi-Yagi antenna was directive along the arm. The end-fire radiation property was added to the previously mentioned quasi-Yagi antenna by using the metasurface unit cells between the human arm and the quasi-Yagi antenna and hence the directivity was enhanced. The geometry of the quasi-Yagi antenna and the metasurface unit cells is shown in Fig. 24 (a) and the radiation pattern and the gain of the same antenna are depicted in Fig. 24 (b), (c), respectively.

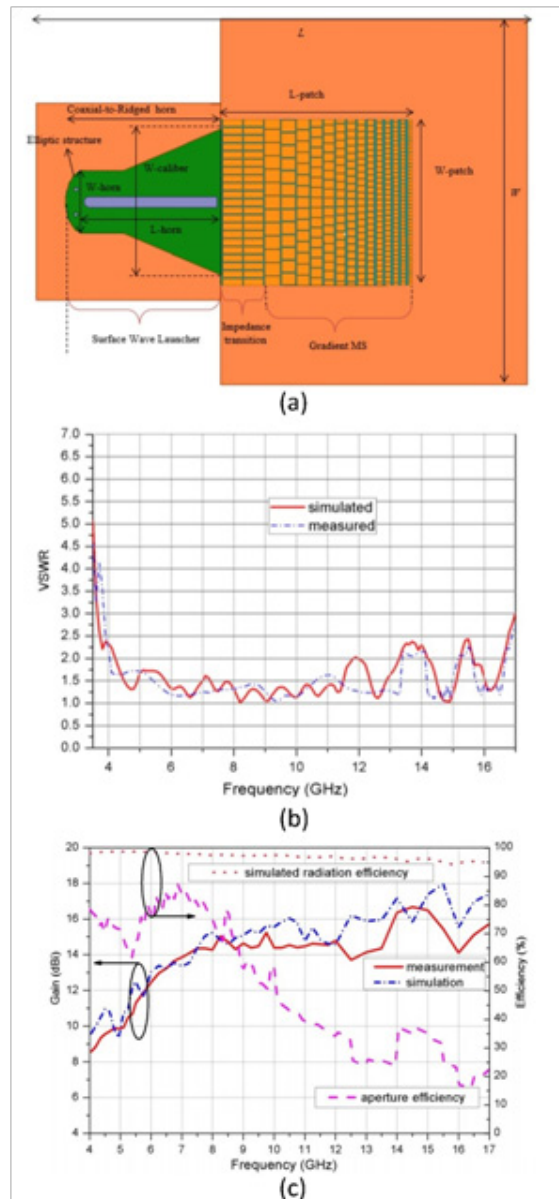


Fig. 25: End-fire antenna loaded with metasurface unit cells to obtain wideband and low profile [67] (a) the geometry of the antenna. (b) VSWR. (c) the gain and efficiency.

A comparison table which indicates the advantage of using metasurface technique than non-metasurface

techniques for end-fire antenna applications is shown below in Table III

Table III: A comparison between Metasurface techniques and other non-Metasurface techniques (end fire antenna)

Ref.	Frequency (GHz)	Fractional BW	Gain (dBi)
77 (non-metasurface)	2	160.6%	7.2-9.2
78 (non-metasurface)	2.5	155.5	3.61-18.7
79 (non-metasurface)	6.9	86.4	9.95-12
80 (metasurface)	3.78	132.3	5.5-14.1
67 (metasurface)	3.8	125.8	8.6-16.67

XI. CONCLUSION

There is a great interest in using the metasurface concept in the antenna community due to its advantages in manipulating electromagnetic waves. The metasurface is made up of two-dimensional scatterers (metallic and dielectric), which make it easy to make and flexible to integrate with other systems. The metasurface unit cells have a size of a sub-wavelength. After introducing generalized Snell's law, a lot of characteristics are obtained by metasurface. Metasurface can be integrated into the antenna community to realize reflectarray antennas and transmit array antennas with high directivity depending

on the anomalous reflection and anomalous refraction concept which is demonstrated by generalized Snell's law. The metasurface can be used also in the Fabry-Perot cavity antenna to increase the directivity and the gain. In stealth technology, metasurface is very important as radar cross-section reduction can be realized. Besides the above applications, the metasurface is used to reduce the mutual coupling between the neighboring antennas especially in array antennas and it is used also to design frequency scanning metasurface antennas. Beamforming and beam splitting are also generated by using metasurfaces.

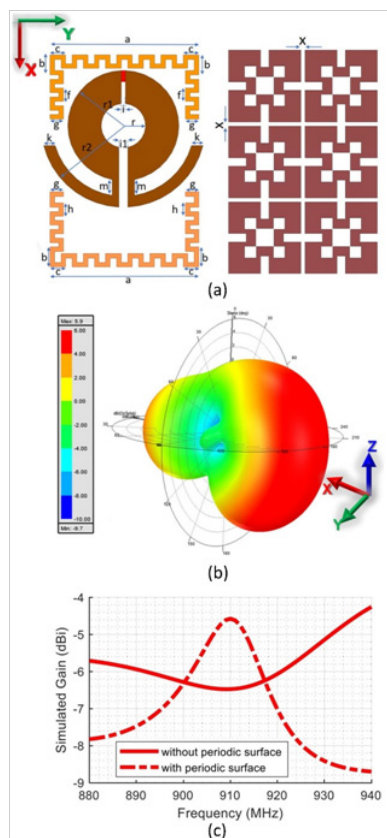


Fig. 26: The quasi-Yagi metasurface antenna^[68] (a) the geometry of the antenna. (b) the metasurface unit cells. (b) the 3-D radiation pattern. (c) the simulated gain with and without metasurface unit cells.

XII. REFERENCES

- [1] C. L. Holloway, E. F. Kuester, J. A. Gordon, J. O'Hara, J. Booth and D. R. Smith, "An Overview of the Theory and Applications of Metasurfaces: The Two-Dimensional Equivalents of Metamaterials," *IEEE Antennas and Propagation Magazine*, vol. 54, no. 2, pp. 10-35, April 2012.
- [2] C. L. Holloway, A. Dienstfrey, E. Kuester, J. O'Hara, A. K. Azad, A. Taylor, "A discussion on the interpretation and characterization of metafilms/metaplanes: The two-dimensional equivalent of metamaterial," *Metamaterials*, vol. 3, pp. 100-112, 2009.
- [3] C. L. Holloway, E. F. Kuester and A. Dienstfrey, "Characterizing Metasurfaces/Metafilms: The Connection Between Surface Susceptibilities and Effective Material Properties," in *IEEE Antennas and Wireless Propagation Letters*, vol. 10, pp. 1507-1511, 2011.
- [4] H. T. Holloway, M. A. Mohamed, E. F. Kuester and A. Dienstfrey, "Reflection and transmission properties of a metafilm: with an application to a controllable surface composed of resonant particles," in *IEEE Transactions on Electromagnetic Compatibility*, vol. 47, no. 4, pp. 853-865, Nov. 2005.
- [5] N. Yu, P. Genevet, M. A. Kats, F. Aieta, J. Tetienne, F. Capasso, Z. Gaburro, "Light Propagation with Phase Discontinuities: Generalized Laws of Reflection and Refraction," *Science*, vol. 334, pp. 333-337, 2011.
- [6] W. Cai, V. Shalaev, *Optical Metamaterials: Fundamentals and Applications* (Springer, 2009) (BOOK)
- [7] N. Engheta, R. W. Ziolkowski, *Metamaterials: Physics and Engineering Explorations* (Wiley/IEEE Press, 2006).
- [8] H. T. Miyazaki, Y. Kurokawa, "Controlled plasmon resonance in closed metal/insulator/metal nanocavities," *Appl. Phys. Lett.* 89, 211126 (2006)
- [9] J. A. Fan *et al.*, "Self-assembled plasmonic nanoparticle clusters," *Science* 328, 1135 (2010)
- [10] R. D. Grober, R. J. Schoelkopf, D. E. Prober, "Optical antenna: Towards a unity efficiency near-field optical probe," *Appl. Phys. Lett.* 70, 1354 (1997).
- [11] J. Huang and J. A. Encinar, *Reflectarray Antennas*. Piscataway, NJ, USA: IEEE Press, 2008.
- [12] S. Sun *et al.*, "High-efficiency broadband anomalous reflection by gradient meta-surfaces," *Nano Lett.*, vol. 12, no. 12, pp. 6223-6229, Dec. 2012
- [13] S. Sun, Q. He, S. Xiao, Q. Xu, X. Li, and L. Zhou, "Gradient-index meta-surfaces as a bridge linking propagating waves and surface waves," *Nature Mater.*, vol. 11, no. 5, pp. 426-431, May 2012.
- [14] A. Díaz-Rubio, V. S. Asadchy, A. Elsakka, and S. A. Tretyakov, "From the generalized reflection law to the realization of perfect anomalous reflectors," *Sci. Adv.*, vol. 3, no. 8, Aug. 2017, Art. no. e1602714.
- [15] S. Yu, L. Li, and G. Shi, "Dual-polarization and dual-mode orbital angular momentum radio vortex beam generated by using reflective metasurface," *Appl. Phys. Express*, vol. 9, no. 8, Aug. 2016, Art. no. 082202
- [16] B. H. Fong, J. S. Colburn, J. J. Ottusch, J. L. Visher, and D. F. Sievenpiper, "Scalar and tensor holographic artificial impedance surfaces," *IEEE Trans. Antennas Propag.*, vol. 58, no. 10, pp. 3212-3221, Oct. 2010.
- [17] Y. Li, X. Wan, B. Cai, Q. Cheng, and T. Cui, "Frequency-controls of electromagnetic multi-beam scanning by metasurfaces," *Sci. Rep.*, vol. 4, no. 1, Nov. 2014, Art. no. 6921.
- [18] S. Sun, Q. He, S. Xiao, Q. Xu, X. Li, L. Zhou, "Gradient-index meta-surfaces as a bridge linking propagating waves and surface waves," *Nature materials*, vol. 11, pp. 426-43, 2012.
- [19] X. Ding, F. Monticone, K. Zhang, L. Zhang, D. Gao, S. N. Burokur, A. Luštrac, Q. Wu, C. Qiu, A. Alù, "Ultrathin Pancharatnam-Berry Metasurface with Maximal Cross-Polarization Efficiency," *Advanced Materials*, vol. 27, pp. 1195-1200, 2015.
- [20] N. Gagnon, A. Petosa, and D. A. McNamara, "Research and development on phase-shifting surfaces (PSSs)," *IEEE Antennas Propag. Mag.*, vol. 55, no. 2, pp. 29-48, Apr. 2013
- [21] A. A. Elsakka, V. S. Asadchy, I. A. Faniayev, S. N. Tsvetkova and S. A. Tretyakov, "Multifunctional Cascaded Metamaterials: Integrated Transmitarrays," in *IEEE Transactions on Antennas and Propagation*, vol. 64, no. 10, pp. 4266-4276, Oct. 2016.
- [22] Z. H. Jiang, L. Kang, W. Hong, and D. H. Werner, "Highly efficient broadband multiplexed millimeter-wave vortices from metasurface-enabled transmit-arrays of subwavelength thickness," *Phys. Rev. A, Gen. Phys.*, vol. 9, Jan. 2018, Art. no. 064009.
- [23] Y. Su and Z. N. Chen, "A flat dual-polarized transformation-optics beamscanning Luneburg lens antenna using PCB-stacked gradient index metamaterials," *IEEE Trans. Antennas Propag.*, vol. 66, no. 10, pp. 5088-5097, Oct. 2018.
- [24] C. Pfeiffer and A. Grbic, "Millimeter-wave transmitarrays for wavefront and polarization control," *IEEE Trans. Microw. Theory Techn.*, vol. 61, no. 12, pp. 4407-4417, Dec. 2013.
- [25] J. Wang *et al.*, "High-efficiency spoof plasmon polariton coupler mediated by gradient metasurfaces," *Appl. Phys. Lett.*, vol. 101, no. 20, Nov. 2012, Art. no. 201104.
- [26] Y. Li *et al.*, "Wideband radar cross section reduction using two-dimensional phase gradient metasurfaces," *Appl. Phys. Lett.*, vol. 104, no. 22, Jun. 2014, Art. no. 221110.
- [27] V. G. Veselago, "The electrodynamics of substances with simultaneously negative values of ϵ and μ ," *Sov. Phys. Uspekhi*, vol. 10, no. 4, pp. 509-514, Apr. 1968.
- [28] H. Chen *et al.*, "Broadband spoof surface plasmon polariton couplers based on transmissive phase gradient metasurface," *J. Phys. D, Appl. Phys.*, vol. 50, no. 37, Sep. 2017, Art. no. 375104.
- [29] H. Li, G. M. Wang, H.-X. Xu, T. Cai, and J. Liang, "X-band phase gradient metasurface for high-gain lens antenna application," *IEEE Trans. Antennas Propag.*, vol. 63, no. 11, pp. 5144-5149, Nov. 2015.
- [30] K. Chen, Z. Yang, Y. Feng, B. Zhu, J. Zhao, and T. Jiang, "Improving microwave antenna gain and bandwidth with phase compensation metasurface," *AIP Adv.*, vol. 5, no. 6, Jun. 2015, Art. no. 067152.
- [31] K. Chen, Z. Yang, B. Zhu and Y. Feng, "Gain and bandwidth enhanced patch antenna with phase compensation metasurface," 2015 IEEE 4th Asia-Pacific Conference on Antennas and Propagation (APCAP), 2015, pp. 267-268.
- [32] S. S. Syed Nasser, W. Liu, and Z. N. Chen, "Wide bandwidth and enhanced gain of a low-profile dipole antenna achieved by integrated suspended metasurface," *IEEE Trans. Antennas Propag.*, vol. 66, no. 3, pp. 1540-1544, Mar. 2018.
- [33] C. Pfeiffer and A. Grbic, "Metamaterial Huygens' surfaces: Tailoring wave fronts with reflectionless sheets," *Phys. Rev. Lett.*, vol. 110, May 2013, Art. no. 197401.
- [34] H. Chen *et al.*, "Ultra-wideband polarization conversion metasurfaces based on multiple plasmon resonances," *J. Appl. Phys.*, vol. 115, no. 15, Apr. 2014, Art. no. 154504.
- [35] X. Fu *et al.*, "Merging bands of polarization converters by suppressing Fano resonance," *Appl. Phys. Lett.*, vol. 113, no. 10, Sep. 2018, Art. no. 101901.
- [36] S. Sui *et al.*, "Absorptive coding metasurface for further radar cross section reduction," *J. Phys. D, Appl. Phys.*, vol. 51, no. 6, Feb. 2018, Art. no. 065603.
- [37] S. Sui *et al.*, "Synthetic design for a microwave absorber and antireflection to achieve wideband scattering reduction," *J. Phys. D, Appl. Phys.*, vol. 52, no. 3, Jan. 2019, Art. no. 035103.
- [38] B. Li, X. Liu, H. Shi, C. Yang, Q. Chen and A. Zhang, "Planar Phase Gradient Metasurface Antenna With Low RCS," *IEEE Access*, vol. 6, pp. 78839-78845, 2018.
- [39] Q. Zheng *et al.*, "Wideband coding metasurfaces based on low Q resonators," *Opt. Commun.*, vol. 430, pp. 189-194, Jan. 2019.
- [40] S. H. Kim and Y. J. Yoon, "Wideband Radar Cross-Section Reduction on Checkerboard Metasurfaces With Surface Wave Suppression," *IEEE Antennas Wireless Propag. Lett.*, vol. 18, no. 5, pp. 896-900, May 2019.
- [41] W. Chen, C. A. Balanis and C. R. Birtcher, "Checkerboard EBG Surfaces for Wideband Radar Cross Section Reduction," *IEEE Trans. Antennas Propag.*, vol. 63, no. 6, pp. 2636-2645, June 2015.
- [42] J. C. Iriarte Galarregui, A. Tellechea Pereda, J. L. M. de Falcón, I. Ederra, R. Gonzalo and P. de Maagt, "Broadband Radar Cross-Section Reduction Using AMC Technology," *IEEE Trans. Antennas Propag.*, vol. 61, no. 12, pp. 6136-6143, Dec. 2013.
- [43] A. Murugesan, D. Natarajan and K. T. Selvan, "Low-Cost, Wideband Checkerboard Metasurfaces for Monostatic RCS Reduction," in *IEEE Antennas and Wireless Propagation Letters*, vol. 20, no. 4, pp. 493-497, April 2021.
- [44] Erik Fritz-Andrade, Angel Perez-Miguel, Ricardo Gomez-Villanueva, Hildeberto Jardón-Aguilar "Characteristic mode analysis applied to reduce the mutual coupling of a four-element patch MIMO antenna using a defected ground structure" *IET Microw. Antennas Propag.*, 2020, Vol. 14 Iss. 2, pp. 215-226.
- [45] K. Wei, J. Li, L. Wang, Z. Xing, and R. Xu, "S-shaped periodic defected ground structures to reduce microstrip antenna array mutual coupling," *Electronics Letters*, vol. 52, no. 15, pp. 1288-1290, 2016.
- [46] S. Ghosh, T. N. Tran, and T. Le-Ngoc, "Dual-Layer EBG-Based



- Miniaturized Multi-Element Antenna for MIMO Systems," *IEEE Transactions on Antennas and Propagation*, vol. 62, no. 8, pp. 3985–3997, Aug. 2014.
- [47] L. Mouffok, L. Damaj, X. Begaud, A. C. Lepage and H. Diez, "Mutual coupling reduction between dual polarized microstrip patch antennas using compact spiral Artificial Magnetic Conductor," *Proceedings of the 5th European Conference on Antennas and Propagation (EUCAP)*, 2011, pp. 909-912.
- [48] H. M. Bernety and A. B. Yakovlev, "Reduction of Mutual Coupling Between Neighboring Strip Dipole Antennas Using Confocal Elliptical Metasurface Cloaks," in *IEEE Transactions on Antennas and Propagation*, vol. 63, no. 4, pp. 1554-1563, April 2015.
- [49] A. Alù, "Mantle cloak: Invisibility induced by a surface," *Phys. Rev. B*, vol. 80, p. 245115, 2009.
- [50] P. Y. Chen, C. Argyropoulos, and A. Alù, "Broadening the cloaking bandwidth with non-foster metasurfaces," *Phys. Rev. Lett.*, vol. 111, p. 233001, 2013.
- [51] A. Dadgarpour, B. Zarghooni, B. S. Virdee, T. A. Denidni and A. A. Kishk, "Mutual Coupling Reduction in Dielectric Resonator Antennas Using Metasurface Shield for 60-GHz MIMO Systems," in *IEEE Antennas and Wireless Propagation Letters*, vol. 16, pp. 477-480, 2017.
- [52] H. Luan, C. Chen, W. Chen, L. Zhou, H. Zhang and Z. Zhang, "Mutual Coupling Reduction of Closely E/H-Plane Coupled Antennas Through Metasurfaces," in *IEEE Antennas and Wireless Propagation Letters*, vol. 18, no. 10, pp. 1996-2000, Oct. 2019.
- [53] J. Tang *et al.*, "A Metasurface Superstrate for Mutual Coupling Reduction of Large Antenna Arrays," in *IEEE Access*, vol. 8, pp. 126859-126867, 2020.
- [54] W. J. Sun, Q. He, S. L. Sun, and L. Zhou, "High-efficiency surface plasmon meta-couplers: Concept and microwave-regime realizations," *Light: Sci. Appl.*, vol. 5, p. e16003, 2016.
- [55] S. Sun and Q. He, "Gradient-index meta-surfaces as a bridge linking propagating waves and surface waves," *Nature Mater.*, vol. 11, pp. 426–431, 2012.
- [56] H. Chen *et al.*, "Wideband Frequency Scanning Spoof Surface Plasmon Polariton Planar Antenna Based on Transmissive Phase Gradient Metasurface," in *IEEE Antennas and Wireless Propagation Letters*, vol. 17, no. 3, pp. 463-467, March 2018.
- [57] Y. Fan *et al.*, "Frequency Scanning Radiation by Decoupling Spoof Surface Plasmon Polaritons via Phase Gradient Metasurface," in *IEEE Transactions on Antennas and Propagation*, vol. 66, no. 1, pp. 203-208, Jan. 2018.
- [58] A. Zhang, R. Yang, D. Li, B. Hu, Z. Lei and Y. Jiao, "Metasurface-Based Tapered Waveguide Slot Array Antennas for Wide Angular Scanning in a Narrow Frequency Band," in *IEEE Transactions on Antennas and Propagation*, vol. 66, no. 8, pp. 4052-4059, Aug. 2018.
- [59] D. Gonzalez-Ovejero, G. Minatti, G. Chattopadhyay, and S. Maci, "Multibeam by metasurface antennas," *IEEE Trans. Antennas Propag.*, vol. 65, no. 6, pp. 2923–2930, Jun. 2017.
- [60] Y. B. Li, R. Y. Wu, W. Wu, C. B. Shi, Q. Cheng, and T. J. Cui, "Dual-physics manipulation of electromagnetic waves by system-level design of metasurfaces to reach extreme control of radiation beams," *Adv. Mater. Technol.*, vol. 2, no. 1, Jan. 2017.
- [61] X. G. Zhang, W. X. Jiang, H. W. Tian, and T. J. Cui, "Controlling radiation beams by low-profile planar antenna arrays with coding elements," *ACS Omega*, vol. 3, no. 9, pp. 10601–10611, Sep. 2018.
- [62] O. Yurduseven and D. R. Smith, "Dual-polarization printed holographic multibeam metasurface antenna," *IEEE Antennas Wireless Propag. Lett.*, vol. 16, pp. 2738–2741, 2017.
- [63] Q. Chen, Z. Hu, Z. Shen, and W. Wu, "2–18 GHz conformal low-profile log-periodic array on a cylindrical conductor," *IEEE Trans. Antennas Propag.*, vol. 66, no. 2, pp. 729–736, Feb. 2018.
- [64] P. Wang, G. Wen, H. Zhang, and Y. Sun, "A wideband conformal endfire antenna array mounted on a large conducting cylinder," *IEEE Trans. Antennas Propag.*, vol. 61, no. 9, pp. 4857–4861, Sep. 2013.
- [65] Z. Hu, Z. Shen, W. Wu, and J. Lu, "Low-profile top-hat monopole Yagi antenna for end-fire radiation," *IEEE Trans. Antennas Propag.*, vol. 63, no. 7, pp. 2851–2857, Jul. 2015.
- [66] P. Wang and Z. Shen, "End-fire surface wave antenna with metasurface coating," *IEEE Access*, vol. 6, pp. 23778–23785, 2018.
- [67] P. Wang, Q. Wu, R. -B. He and Y. Shao, "Design of Low Profile and Wideband End-Fire Antenna Using Metasurface," in *IEEE Access*, vol. 8, pp. 35752-35758, 2020.
- [68] S. Ahmed, D. Le, L. Sydänheimo, L. Ukkonen and T. Björninen, "Wearable Metasurface-Enabled Quasi-Yagi Antenna for UHF RFID Reader With End-Fire Radiation Along the Forearm," in *IEEE Access*, vol. 9, pp. 77229-77238, 2021.
- [69] J. -W. Lian, Y. -L. Ban and Y. J. Guo, "Wideband Dual-Layer Huygens' Metasurface for High-Gain Multibeam Array Antennas," in *IEEE Transactions on Antennas and Propagation*, vol. 69, no. 11, pp. 7521-7531, Nov. 2021.
- [70] Y. Fu, J. Ji, Y. Wang, F. Zhou, C. Wang and P. Chen, "Broadband radar cross section reduction binary metasurface with a high-efficiency intraband transmission window," in *IEEE Antennas and Wireless Propagation Letters*.
- [71] Y. FU, Y. Li, N. Yuan, "Wideband composite AMC surfaces for RCS reduction," *Microw. Opt. Technol. Lett.*, vol. 53, pp.712-715, 2011.
- [72] J. C. Iriarte Galarregui, A. Tellechea Pereda, J. L. M. de Falcón, I. Ederria, R. Gonzalo and P. de Maagt, "Broadband Radar Cross-Section Reduction Using AMC Technology," in *IEEE Transactions on Antennas and Propagation*, vol. 61, no. 12, pp. 6136-6143, Dec. 2013.
- [73] W. Chen, C. A. Balanis and C. R. Birtcher, "Dual Wide-Band Checkerboard Surfaces for Radar Cross Section Reduction," in *IEEE Transactions on Antennas and Propagation*, vol. 64, no. 9, pp. 4133-4138, Sept. 2016.
- [74] K. S. Vishvaksenan, K. Mithra, R. Kalaiarasan, and K. S. Raj, "Mutual coupling reduction in microstrip patch antenna arrays using parallel coupled-line resonators," *IEEE Antennas Wireless Propag. Lett.*, vol. 16, pp. 2146–2149, 2017
- [75] K. S. Vishvaksenan, K. Mithra, R. Kalaiarasan, and K. S. Raj, "Mutual coupling reduction in microstrip patch antenna arrays using parallel coupled-line resonators," *IEEE Antennas Wireless Propag. Lett.*, vol. 16, pp. 2146–2149, 2017.
- [76] Z. Qamar, U. Naeem, S. A. Khan, M. Chongcheawchamnan, and M. F. hafique, "Mutual coupling reduction for high-performance densely packed patch antenna arrays on finite substrate," *IEEE Trans. Antennas Propag.*, vol. 64, no. 5, pp. 1653–1660, May 2016.
- [77] Q. Chen, Z. Hu, Z. Shen and W. Wu, "2–18 GHz Conformal Low-Profile Log-Periodic Array on a Cylindrical Conductor," in *IEEE Transactions on Antennas and Propagation*, vol. 66, no. 2, pp. 729-736, Feb. 2018.
- [78] P. Wang, Q. Wu, R. -B. He and W. Luo, "Gain and Radiation Pattern Enhancement of the H-Plane Horn Antenna Using a Tapered Dielectric Lens," in *IEEE Access*, vol. 7, pp. 69101-69107, 2019.
- [79] Z. Hu, S. Cao, M. Liu, C. Hua and Z. Chen, "A Planar Low-Profile Log-Periodic Array Based on Cavity-Backed Slot," in *IEEE Antennas and Wireless Propagation Letters*, vol. 18, no. 10, pp. 1966-1970, Oct. 2019.
- [80] P. Wang and Z. Shen, "End-Fire Surface Wave Antenna With Metasurface Coating," in *IEEE Access*, vol. 6, pp. 23778-23785, 2018.